Article

Neuron

Synapse-Level Determination of Action Potential Duration by K^+ Channel Clustering in Axons

Highlights

- Spike duration varies between presynaptic boutons within an individual SC axon
- The varicose geometry of presynaptic boutons does not alter spike duration
- Fast-activating K^+ channels are clustered at boutons and restricted from shafts
- AP duration is determined by K_v3 channels immediately local to an individual bouton

Authors

Matthew J.M. Rowan, Gina DelCanto, Jianqing J. Yu, Naomi Kamasawa, Jason M. Christie

Correspondence

jason.christie@mpfi.org

In Brief

Rowan et al. find that APs are not uniformly represented across the axon arbor of SCs. Rather, spike duration is subject to local variation, determined at individual release sites, by clustering of fast-activating K^+ channels, thus contributing to release heterogeneity.

Rowan et al., 2016, Neuron *91*, 370–383
July 20, 2016
http://dx.doi.org/10.1016/j.neuron.2016.05.035

CellPress

CellPress

Neuron
Article

Synapse-Level Determination of Action Potential Duration by K^+ Channel Clustering in Axons

Matthew J.M. Rowan,[1] Gina DelCanto,[2,3] Jianqing J. Yu,[1] Naomi Kamasawa,[1] and Jason M. Christie[1,*]
[1]Max Planck Florida Institute for Neuroscience, Jupiter, FL 33458, USA
[2]Wilkes Honors Campus of Florida Atlantic University, Jupiter, FL 33405, USA
[3]Current address: Biochemistry Graduate Program, University of Miami, Miami, FL 33136, USA
*Correspondence: jason.christie@mpfi.org
http://dx.doi.org/10.1016/j.neuron.2016.05.035

SUMMARY

In axons, an action potential (AP) is thought to be broadcast as an unwavering binary pulse over its arbor, driving neurotransmission uniformly at release sites. Yet by recording from axons of cerebellar stellate cell (SC) interneurons, we show that AP width varies between presynaptic bouton sites, even within the same axon branch. The varicose geometry of SC boutons alone does not impose differences in spike duration. Rather, axonal patching revealed heterogeneous peak conductance densities of currents mediated mainly by fast-activating K_v3-type potassium channels, with clustered hotspots at boutons and restricted expression at adjoining shafts. Blockade of K_v channels at individual boutons indicates that currents immediately local to a release site direct spike repolarization at that location. Thus, the clustered arrangement and variable expression density of K_v3 channels at boutons are key determinants underlying compartmentalized control of AP width in a near synapse-by-synapse manner, multiplying the signaling capacity of these structures.

INTRODUCTION

Spike width has a profound influence on neurotransmission, for the action potential (AP) is the command waveform directing Ca_v channel opening, and release probability is steeply dependent on Ca^{2+} concentration (Borst and Sakmann, 1999; Sabatini and Regehr, 1997). Recent work has shown that AP shape, determined in part by K^+-mediated currents, may be adaptively regulated with Ca_v channel abundance (Hoppa et al., 2012, 2014). That Ca_v channels are organized in a synapse-specific manner is well-appreciated (Holderith et al., 2012; Sheng et al., 2012). Yet the AP is classically viewed as a monotypic binary pulse transmitted throughout the entire extent of an axon, obviating synapse-level control of AP width. Despite this simplistic view, axons achieve a high degree of specificity in the organization and functional influence of both Na_v and K_v channels to impart compartmentalized control of membrane excitability within their structure (Debanne et al., 2011). For example, the restricted abundance of Na_v channels at terminal release sites has been shown to attenuate APs, in part, defining release probability and contributing to short-term plasticity (Kawaguchi and Sakaba, 2015; Leão et al., 2005; Wu et al., 2004).

Unlike the terminal endings of projection neurons, APs in axons of local interneurons encounter frequent presynaptic boutons arranged en passant whose morphology and molecular composition may impose a highly localized alteration in waveform as the spike propagates from one release site to the next, yet this remains relatively unexplored. More broadly, quantitative measurements from the axons of CNS interneurons indicate that AP signaling is regulated by a non-uniform subcellular organization of Na_v and K_v channels. In fast-spiking hippocampal interneurons, Na_v channel density scales with distance from the soma to ensure fast and reliable AP propagation in an extensively branching arbor (Hu and Jonas, 2014). In cerebellar stellate cells (SCs), spike repolarization is differentially tuned by distinct K_v channel types at the axon initial segment (AIS) and presynaptic boutons, limiting use-dependent spike broadening to the AIS (Rowan et al., 2014). Therefore, it is likely that representation of the AP within an axon may be more heterogeneous than previously thought, influenced by the types and availability of ion channels at any particular region.

Here, using methods to directly sample APs at different locations within the same axon of cerebellar SCs, we find that spike width varies between presynaptic boutons. Spike repolarization is driven by fast-activating K_v3-type channels whose clustered organization at release sites allows APs to be shaped by the K^+ conductance immediate local at one bouton site, independent of other sites. Together, our results point to a much broader functional signaling repertoire for APs in axons where differences in spike width contribute to the heterogeneity of release efficacy, thus multiplying the signaling range of these structures.

RESULTS

AP Width Varies between Axonal Boutons

We studied the functional properties of SC axons in acute cerebellar slices using targeted subcellular recording. To visualize axons, SCs were filled somatically during whole-cell recording with a fluorescent dye and imaged with two-photon (2P) microscopy. The boutons of labeled axons were optically targeted for loose-seal patch recording under continuous imaging using fluorescent pipettes (Sasaki et al., 2012) (Figure 1A). Somatically

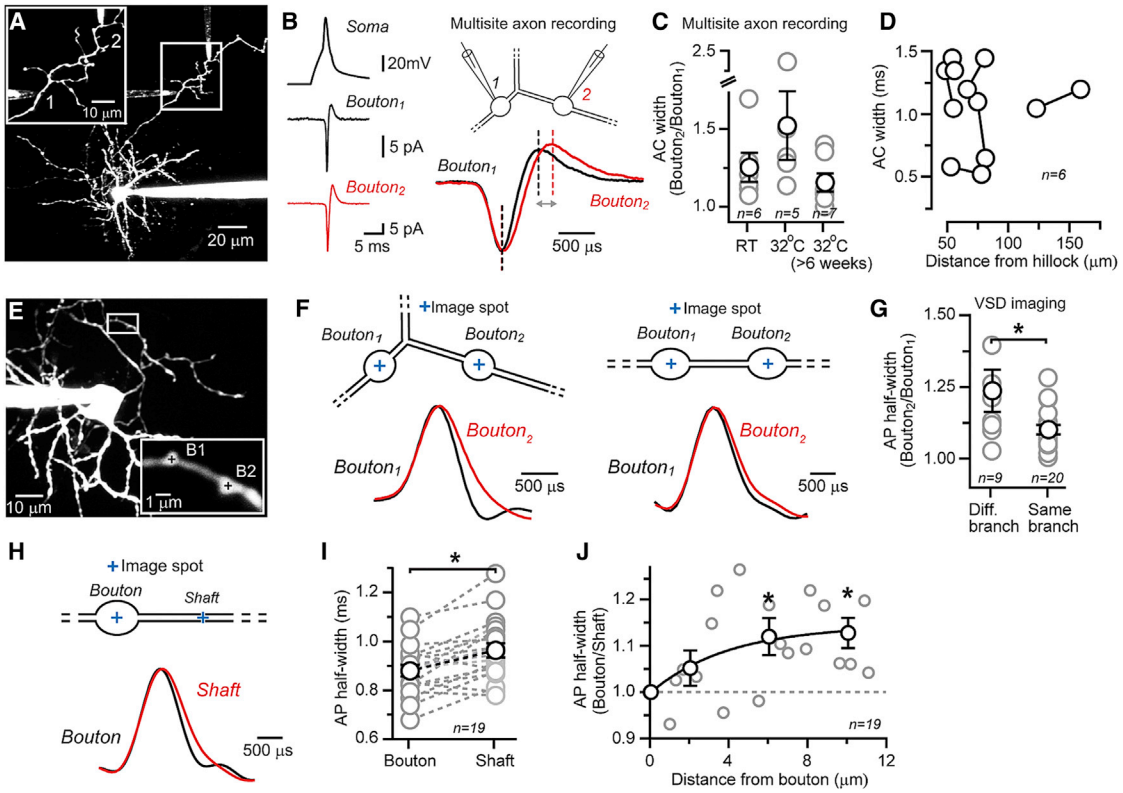

Figure 1. Variable Spike Width in SC Axons

(A) 2P fluorescence image of an SC (Alexa 594; 60 µM) with simultaneous loose-seal recordings from two boutons on separate axon branches.

(B) Axonal action currents were elicited by somatically evoked APs. In the enlarged view, superimposed currents are aligned by the peaks of their inward components with the width difference indicated by the double-headed gray arrow.

(C) Group data summary of action current (AC) width comparisons for multisite axon recordings. Differences in width are expressed as a ratio between same-cell measurement locations. Conditions were not significantly different from one another ($p > 0.05$; one-way ANOVA with Tukey's multiple comparison test).

(D) Action current widths are plotted for multisite axon recordings as a function of distance from the axon hillock. Same-cell measurements from a common axon are connected (mean distance between boutons 28.3 µm; range 9.2–46.8 µm; ≥1 branch between sites).

(E) Representative SC image with bouton VSD recording sites depicted in the inset.

(F) APs recorded with 2P VSD imaging from two boutons on the same axon. Examples are shown from boutons separated by a branch point (left) or near neighbors on the same branch (right).

(G) Summary data for multisite VSD imaging of boutons (different branch [≥1 branch between sites], mean distance 24.9 µm, range 19.9–52.5 µm; and same branch, mean distance 5.9 ± 0.8 µm, range 1.0–11.1 µm). Spike width varied to a greater extent between boutons located on separate branches (*$p = 0.03$; Mann-Whitney test).

(H) APs from a bouton as well as a site on the connecting shaft recorded using 2P VSD imaging.

(I) Relative to their adjoining bouton, APs in shafts were broader in duration (*$p < 0.0001$; paired t test; mean distance between recording locations 5.9 ± 0.8 µm).

(J) Orthodromic AP broadening in axon shafts depends on distance from the bouton. A monoexponential fit to grouped data (4 µm bins) yielded a length constant (λ) of 3.9 µm (*$p < 0.05$; one-way ANOVA with Dunnett's multiple comparison test).

For all summary graphs, data are expressed as mean (±SEM) and shown in black with individual data points in gray. See also Figure S1.

elicited APs were resolved in the axon as rapid action currents with inward and outward components corresponding to the depolarizing and repolarizing phase of the underlying AP, respectively. The peak-to-peak timing of these components closely approximates AP half-width (Rowan et al., 2014; Sabatini and Regehr, 1997; Sasaki et al., 2011; Yang and Wang, 2006). Using two axonal electrodes, simultaneous recordings were obtained from boutons located on nearby branches (Figures 1A and 1B). Comparison of axonal action currents revealed considerable variability in duration between recording sites (Figures 1B and 1C), independent of bouton order or distance from the soma (Figure 1D), indicating that the rate of AP repolarization is not constant within an axon. Action current duration was unchanged during repetitive spiking (20 Hz; Figures S1A and S1B, available online), suggesting that differences persist despite ongoing suprathreshold activity. Differences in AP duration between recording sites were also observed at near-physiological temperature (32°C), in mature mice (>6 weeks old and 32°C; Figure 1C), and during spontaneous firing (16.2 ± 2.7 Hz; Figures S1C and S1D).

In a separate set of experiments, we used voltage-sensitive dye (VSD) imaging to record APs at several axon locations. After filling with the VSD di-2-AN(F)EPPTEA (Acker et al., 2011) during whole-cell recording (Figure 1E), somatically evoked APs were

resolved in axons at high temporal resolution from diffraction-limited points of interest with non-scanning 2P excitation (Rowan et al., 2014). Similar to electrophysiological measurements, spike width varied between boutons located on separate branches (Figures 1F and 1G), with the average absolute difference in AP duration comparable with both methods (0.21 ± 0.06 and 0.19 ± 0.04 ms; p = 0.94; unpaired t test; patch recording and VSD imaging, respectively). Unlike electrode recording, 2P VSD imaging allows for targeted subcellular recording without spatial constraint, including boutons within the same axon branch (Figure 1E). In paired measurements from within-branch boutons, variability in AP width was also apparent (Figures 1F and 1G), despite their close apposition. However, spike width was less variable relative to measurements from boutons belonging to different branches (Figure 1G), indicating increased regional homogeneity in AP repolarization rate within individual axon branches.

To assess the spatial extent by which spike width is locally determined within an axon branch, we used VSD imaging to record APs in both a bouton and its outwardly connecting shaft (Figure 1H). In this comparison, we biased recordings to relatively isolated bouton-shaft pairs where the next apparent bouton on the branch was >5 μm distal to the shaft recording location. Orthodromic APs were consistently broader in duration in shafts relative to boutons (Figure 1I), indicating that differences in AP width within an axon branch are not a simple reflection of random variability. As APs propagated from boutons into shafts, broadening occurred in a distance-dependent manner with a length constant (λ) of 3.9 μm (Figure 1J). Together, these results demonstrate that AP width within SC axons is not uniform. Rather, spike duration varies on an exquisitely fine spatial scale, indicating a high degree of compartmentalization in determination of AP repolarization rate.

Axonal Geometry and AP Width

If AP width is not uniform in an axon, then there must be local attributes that impose alteration of spike shape. As APs course through axons, they encounter complex geometric features, including frequent branch points and varicose enlargements at presynaptic boutons where discontinuities in impedance may alter spike propagation (Goldstein and Rall, 1974; Lüscher and Shiner, 1990). To assay how the relative geometric relationship of boutons and their adjoining shafts affects the width of a spike, we used compartmental modeling with simulated APs. To constrain our model, we quantified the structural details of SC axons using three-dimensional reconstructions from serial-section electron microscopy (EM) images (Figure S2). Notably, in these images there was no obvious oligodendrocyte ensheathment of shafts, indicating that SC axons are unmyelinated.

From these ultrastructural measurements, we developed a simplified compartmental model of an SC axon with reduced morphological complexity (Figure 2A); however, the diameters of shafts and boutons were constrained by mean values obtained from EM analysis (153 and 374 nm for shafts and boutons, respectively; Table S1). Within a test region containing a single bouton-shaft pair (Figure 2A), the geometric ratio (Segev and Schneidman, 1999) (GR) varied with bouton diameter (range 244–804 nm; e.g., GR = 3.8, mean bouton diameter). Axons were populated with uniform arrangements of fast-activating Na_v and K_v channels (Engel and Jonas, 2005; Lien and Jonas, 2003), resulting in APs with durations (802–857 μs) similar to our experimental measurements. Analysis of AP duration over a range of realistic GR values indicated that axonal geometry modestly contributes to local width changes of spikes in SC axons (Figures 2B and 2C). However, even the largest geometric mismatches between boutons and shafts (GR ≥ 12) failed to recapitulate our experimental observations.

We sought to experimentally assess whether AP duration is related to axonal geometry by comparing the spike widths of two boutons on the same branch, recorded using VSD imaging, to their relative volumetric difference. As structural features of SC axons approach the resolution limit of 2P microscopy, we used the fluorescence intensity of a chromatically compatible inert intracellular dye (Oregon Green 488) as measure of bouton volume (Svoboda, 2004). However, differences in AP width did not co-vary with bouton size (Figure 2D). As a second approach, we experimentally imposed an increase in GR between boutons and shafts and measured for an accompanying change in AP width. Perfusion of a hyposmotic extracellular solution induced rapid (~30 s) enlargements of axonal structures (Babila et al., 1990; Pullarkat et al., 2006) with a greater volume change in boutons relative to shafts (Figures 2E and 2F). Despite an apparent GR increase, AP width was unaffected (Figure 2G; 1.07% ± 0.04% of control, n = 8, p = 0.12; paired t test). Together, these results suggest that impedance mismatches alone, determined by the variable geometry of varicose boutons and their attached axon shafts, do not account for the local differences in AP width within axons of SCs.

K_v3 Channels Contribute to Variability of AP Width

An emerging view suggests that axons are composed of discrete functional domains whose excitability is each determined by the unique complement of channels specific to that region (Debanne et al., 2011). In SCs, K_v3-type channels direct spike repolarization at boutons, but not the AIS, indicating a regional influence of these channels in the control of spike signaling (Rowan et al., 2014). We examined the possibility that the select influence of K_v3 channels at boutons imparts control of spike repolarization on a much finer spatial scale, thus contributing to differences in AP width within and between axon branches. As previously reported (Rowan et al., 2014), bath application of the K_v3 channel modulator BDS-I (Yeung et al., 2005) or the blocker TEA (Coetzee et al., 1999; Ishikawa et al., 2003) broadened APs in boutons (Figures 3A and 3B) measured with VSD imaging. Surprisingly, APs were unaffected in axon shafts (Figures 3A and 3B), suggesting a bouton-specific role for K_v3-mediated currents in determining spike repolarization. This location-dependent effect of TEA reduced the difference in AP width between boutons and connecting shafts (Figures 3C and 3D). The normalizing effect of TEA was not due to technical errors related to VSD imaging (Figure S3). Furthermore, AP width became more uniform between boutons in TEA when measured with either VSD imaging or loose-seal recording (Figures 3E–3H). Thus, in the absence of K_v3-mediated currents, spike duration is less variable in SC axons, directly implicating these channels in subregional control of AP width.

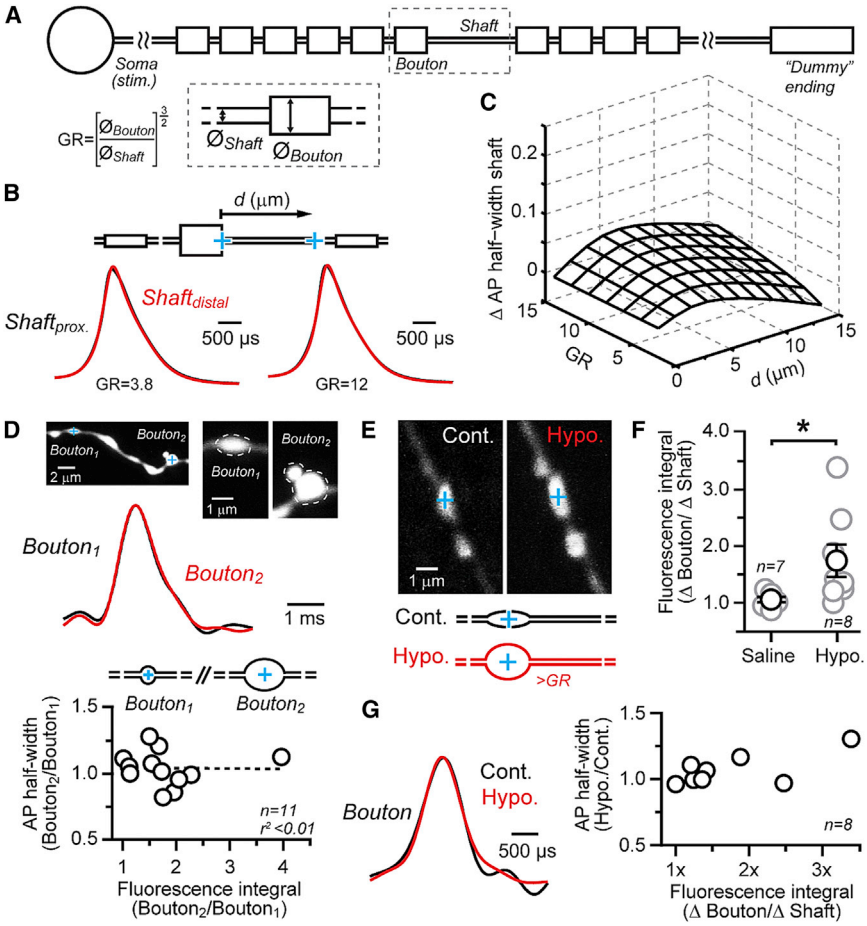

Figure 2. Effect of Axon Geometry on AP Width

(A) Schematic representation of the simplified compartmental model of an SC axon used for simulations with the test bouton and axon shaft demarcated in the boxed region.

(B) Simulated APs from the axon shaft including a proximal location immediately adjacent to the test bouton are shown superimposed for two different GR conditions.

(C) 3D plot showing minimal AP broadening in the axon shaft as a function of increasing GR and distance from the test bouton.

(D) APs recorded with 2P VSD imaging from two different-sized boutons within a branch. Grouped data showing ratio of AP widths recorded from two boutons on the same axon branch plotted against ratio of their relative fluorescence intensity, an approximate measure of volume. A linear regression fit to the data did not deviate from zero ($p = 0.96$; runs test).

(E) Images of an axon branch (Oregon Green 488; 20 μM) before and after perfusion of hypotonic external solution.

(F) Hypotonic swelling induces a larger fluorescence change in boutons relative to axon shafts, indicative of a disproportional volume increase and hence a greater GR. Data are expressed as mean (±SEM); individual data points shown in gray (*$p = 0.04$; unpaired t test).

(G) Superimposed APs, measured in the same bouton using 2P VSD imaging, in control and following hypotonic swelling. VSD imaging locations are depicted by the crosshairs in the fluorescence images. In the summary graph, AP width in boutons remained unaffected despite geometric alteration ($p = 0.07$; F test, wherein slope = 0 for the null hypothesis).

See also Figure S2 and Table S1.

Non-uniform K^+ Conductance Density in Axons

The location-specific role of K_v3 channels in determining AP repolarization specifically at boutons is indicative of a high degree of K^+ channel organization within SC axons. To functionally evaluate voltage-gated K^+ channel activity, we measured pharmacologically isolated K^+ currents in axons in the cell-attached recording configuration (membrane seal resistance 13.4 ± 1.2 GΩ; n = 98) obtained using small open-tip diameter pipettes (Figures S4A and S4B). Cells were simultaneously voltage clamped at the soma (−80 mV) during axonal recordings to mitigate changes in intracellular membrane potential induced by maximally activating voltage pulses elicited by the axon-attached pipette (Williams and Wozny, 2011). Depolarization of the axonal patch evoked fast K^+ currents ($\tau < 2$ ms) in most boutons (13 of 19 patches; $p < 0.05$; one-sample z test; Figures 4A and 4C), whereas in shafts, patches with fast outward currents were rare (2 of 13 patches; $p > 0.05$; one-sample z test). Accordingly, the average activation rate (τ) of K^+ currents was slower in shafts compared to boutons (Figure 4C). A barely discernable conductance attributable to an unknown K^+ channel type was apparent in many shaft recordings and in the few bouton patches lacking fast currents (Figures 4A–4C). To convert currents to conductance density ($\bar{g}_{K^+}$), we determined patch area with capacitance measurements (Figures S4C and S4D). Peak $\bar{g}_{K^+}$ was highly variable in boutons (coefficient of variation [CV] = 144%), with $\bar{g}_{K^+}$ exceeding 100 mS·cm^{-2} in some measurements (Figure 4D). On average, $\bar{g}_{K^+}$ was greater in boutons compared to shafts (Figures 4A and 4D).

In a subset of data presented above, we used a non-morphological method to demarcate putative release sites for targeted patching. Molecular layer interneurons, including SCs, were virally transduced in vivo with high specificity (Figure 4E) with the vesicular protein synaptophysin tagged with YFP (Syph-YFP; Figure 4F). Syph-YFP was segregated to small punctate areas of SC axons, usually corresponding to varicose bouton swellings (Figure 4F). When patch recordings were targeted to varicose axonal sites expressing Syph-YFP, fast-activating K^+ currents were encountered in most patches ($\tau < 2$ ms, 5 of 7 patches; $p < 0.05$; one-sample z test; Figure 4G). In patches lacking Syph-YFP sampled from non-varicose axon areas, fast-activating currents were seldom encountered ($\tau < 2$ ms, 1 of 5 patches; $p > 0.05$; one-sample z test) and $\bar{g}_{K^+}$ was significantly less than at Syph-YFP sites (Figures 4G and 4H). Together, these observations indicate a non-uniformity of K^+ currents in SC axons, with clusters of fast-activating channels at bouton release sites and their restriction from shafts.

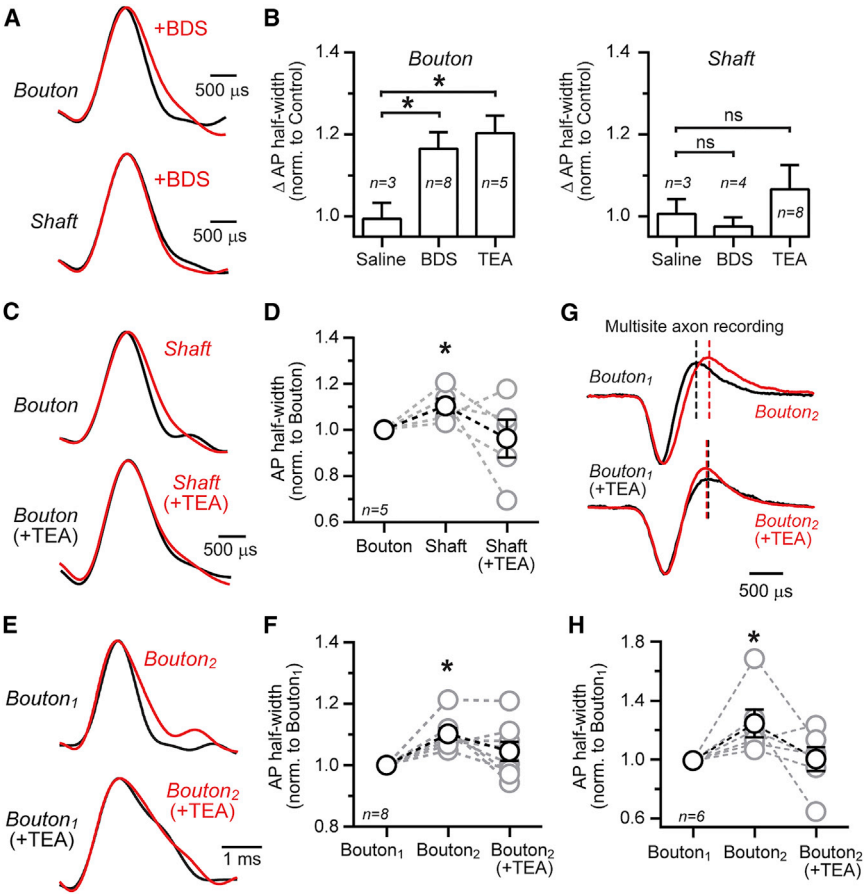

Figure 3. Uniform Spike Duration in Axons in the Absence of K_v3 Currents

(A) Superimposed APs, measured with 2P VSD imaging, in control and following bath application of BDS-1 (1 µM) in either a bouton or a shaft.

(B) Summary graphs show that BDS-1 and TEA increase AP duration in boutons, but not shafts (*p < 0.05; one-way ANOVA with Tukey's multiple comparison test). Measurement locations on shafts were ≥5 µm from adjacent boutons. Data are expressed as mean ± SEM.

(C) Paired AP measurements from a bouton and adjoining shaft in control and following application of TEA (500 µM).

(D) Differences in AP width observed with 2P VSD between boutons and adjoining shafts were reduced by TEA (*p < 0.05).

(E) APs, measured from two boutons on the same branch, in control and following TEA.

(F) In TEA, spike width differences between boutons were no longer significant (*p < 0.05).

(G) Action currents recorded in boutons from different branches in control and following TEA.

(H) TEA reduced action current width differences between boutons (*p < 0.05).

Significance determined with one-way ANOVA followed by Dunnett's multiple comparison test (D, F, and H). Mean data values (±SEM) are presented in black with individual data points shown in gray. See also Figure S3.

K_v3-Mediated Currents at Boutons

For pinceau terminals of basket cell molecular layer interneurons, fast-activating K^+ currents are likely mediated by a combination of both K_v1 and K_v3 channels (Southan and Robertson, 2000), similar to the calyx of Held and mossy fiber boutons in the hippocampus and cerebellum (Alle et al., 2011; Ishikawa et al., 2003; Ritzau-Jost et al., 2014). To study the potential contribution of K_v3 channels in SC boutons, we pharmacologically inhibited K_v1 channels by inclusion of dendrotoxin-I (DTX) (Alle et al., 2011) in the axonal patch pipette. Fast-activating currents were encountered in bouton patches during maximally activating depolarizing pulses, although infrequently (Figure 5A; 9 of 19; $p > 0.05$; one-sample z test), suggestive that pharmacological separation by channel type may reveal a more elaborate clustered arrangement of channels on the bouton membrane. For biophysical analyses, we used a selection criterion rejecting patches with slow activation kinetics ($\tau > 2$ ms), which correlated with negligible current density (Figure S5A). For pharmacologically isolated K_v3-mediated currents, activation was rapid for maximally activating pulses (Figure S5B; $\tau = 0.59 \pm 0.07$ ms; $n = 9$) with a midpoint potential similar to that of K_v3 currents in both inhibitory interneurons and hippocampal mossy fiber boutons (Alle et al., 2011; Lien and Jonas, 2003) (Figure 5B; $V_{half} = -14.6$ mV; $n = 4$).

In fast-spiking interneurons, K_v3 channels may result from the co-assembly of both $K_v3.1$ and $K_v3.4$ subunits (Baranauskas et al., 2003), with the composite current activation profile reflecting the influence of both channel types. Using $Kv3.1^{-/-}$ knockout (KO) mice (Ho et al., 1997), K_v3-mediated currents exhibited a negative shift in activation voltage compared to wild-type (WT) mice (Figure 5B; $V_{half} = -38.0$ mV; $n = 4$), in agreement with the observation that channels composed of $K_v3.1$ subunits activate at more positive voltages (Baranauskas et al., 2003). Correspondingly, in boutons of $Kv3.4^{-/-}$ KO mice, currents had a positive shift in the midpoint of activation (Figure 5B; $V_{half} = -2.9$ mV; $n = 5$), in keeping with the more negative activation range of $K_v3.4$ channels (Baranauskas et al., 2003). Additionally, when compared to WT mice, K_v3-mediated mean peak $\bar{g}_{K^+}$ (Figure 5D) was reduced in both $Kv3.1^{-/-}$ (64.5 ± 16.4 mS·cm^2; $n = 6$; $p = 0.03$; Mann-Whitney test) and in $Kv3.4^{-/-}$ KO mice (59.9 ± 29.3 mS·cm^2; $n = 5$; $p = 0.03$; Mann-Whitney test).

Having functionally identified constituent subunits of K_v3 channels, we sought to further examine for the possibility of clustered arrangements of these channels in SC axons. Therefore, we virally transduced SCs with YFP-tagged $K_v3.4$ subunits ($K_v3.4$-YFP). Despite overexpression, we observed punctate $K_v3.4$-YFP fluorescence along the axon localized at boutons (Figure S6A), the level of which was only weakly correlated

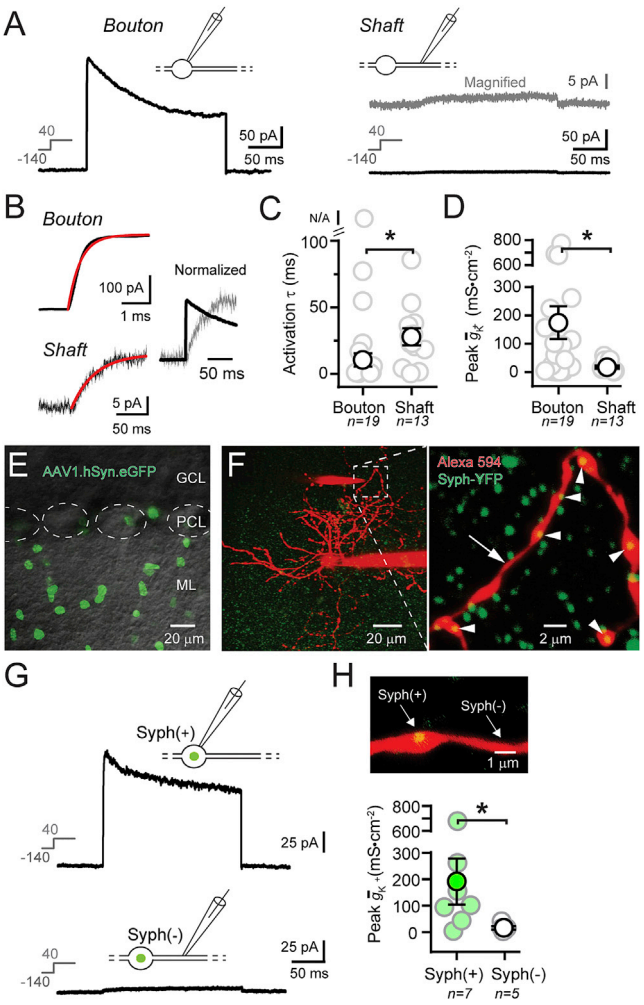

Figure 4. Clustering of Fast-Activating K^+ Currents at Boutons

(A) A fast-activating K^+ current in a bouton patch evoked by a depolarizing pulse (200 ms; preceded by prepulse hyperpolarization to −140 mV for 200 ms). In a shaft recording, depolarization resulted in a slowly activating negligible current. A magnified view of the same record is shown in gray. The whole-cell somatic pipette is not included in the schematic representations of the recording configuration.

(B) Monoexponential fits to K^+ currents recorded in a bouton and a shaft. For comparison, peak-normalized currents are also shown superimposed on the same timescale.

(C) Pooled data showing that bouton patches had fast-activating K^+ currents. One bouton patch with negligible K^+ currents could not be fit with a monoexponential (*p = 0.02; Mann-Whitney test).

(D) Pooled summary data showing boutons have a greater peak K^+ conductance density than shafts (*p = 0.03; Mann-Whitney test).

(E) 2P image of a cerebellar slice taken from a mouse previously injected with AAV1.hSyn-eGFP. Fluorescently labeled cell bodies are found predominately in the molecular layer (ML), consistent with widespread expression in both basket and stellate cells driven by viral serotype and promoter specificity. ML, molecular layer; PCL, Purkinje cell layer; GCL, granule cell layer.

(F) A virally transduced SC expressing YFP-tagged synaptophysin (Syph-YFP; AAV1.hSyn.Syph-YFP). The cell has been filled with the volumetric indicator Alexa 594 (60 µM) during whole-cell recording to visualize the axon. In the magnified view taken prior to axon patching, punctate Syph-YFP fluorescence is visible throughout the axon (arrowheads) marking putative sites of release. Generally, YFP fluorescence coincided with bouton varicosities. Short axon regions lacking YFP fluorescence were also apparent (arrow). Syph-YFP is also expressed surrounding molecular layer interneurons.

(G) Cell-attached recordings from patches of axon in regions with or without Syph-YFP fluorescence. K^+ currents were evoked by short depolarizing pulses (200 ms).

(H) Subset of patch data from Syph-YFP expressing SCs showing K^+ currents at release sites were variable but generally had a high conductance density. In contrast, patches from non-synaptic regions had much lower peak K^+ conductance values. Significance (*p = 0.03) was determined with a Mann-Whitney test. In the summary graph, mean values (±SEM) are shown in black with data from individual patches in gray outline. For all synaptophysin-targeted recordings, mice were >PND 42.

See also Figure S4.

with bouton volume (Figure S6B). Notably, the fluorescence intensity of puncta varied considerably between neighboring sites (Figure S6C), suggesting that subunit composition or abundance is not uniform across boutons.

K_v3-Mediated Currents Are Predominant during APs

Although a pure K_v3 channel blocker is unavailable, low-concentration TEA (1 mM) inhibits K_v3 with high selectivity while keeping K_v1 channels relatively unblocked (Coetzee et al., 1999; Ishikawa et al., 2003), including DTX-sensitive channels expressed in SCs (Rowan et al., 2014). Fast-activating currents were apparent in a minority of recordings with TEA (Figure 5A; 8 of 17 patches; $p > 0.05$; one-sample z test). Examining these putative K_v1 currents, mean peak $\bar{g}_{K^+}$ was significantly reduced compared to measurements in DTX, indicating that the K_v3-mediated conductance likely predominates at boutons (Figure 5D). K_v1 channels typically activate at lower voltages than K_v3 (Dodson and Forsythe, 2004). Accordingly, in TEA, currents were shifted to lower activation voltages (Figure 5B; V_{half} = −32.1 mV; n = 5) with respect to K_v3 currents measured in DTX. Fast-activating K^+ currents were absent when both DTX and TEA were included in the cell-attached pipette (Figure 5A; 8 of 8 patches). Thus, these results indicate that although both K_v1 and K_v3 channels are expressed at boutons, K_v3-mediated currents are the major voltage-activated K^+ conductance at these presynaptic sites.

To determine the current contribution of these K^+ channel types during an AP, we drove channel opening from a physiological membrane potential with an AP-like voltage waveform kinetically similar to an axonal spike measured with VSD imaging (+30 mV peak). Peak $\bar{g}_{K^+}$ was substantially greater for pharmacologically isolated K_v3 currents than for those mediated by putative K_v1 channels (Figures 5E and 5F), indicating that during spiking, the K_v3-mediated conductance is overwhelmingly predominant. The relative recruitment of available K_v1 and K_v3 channels by a spike, determined by comparing currents evoked by the AP-like waveform to those of a square pulse to a maximally activating potential (Baranauskas et al., 2003; Martina et al., 2007) (Figure 5G), was similar in both channel types (23.8% ± 7.5% and 16.6% ± 3.4%; K_v1 and K_v3, respectively; p = 0.94; Mann-Whitney test). Because K_v3 and K_v1 currents displayed similar activation kinetics at suprathreshold voltages (Figures S5B and S5C), the predominant recruitment of K_v3-mediated currents during an AP likely results from their greater relative availability.

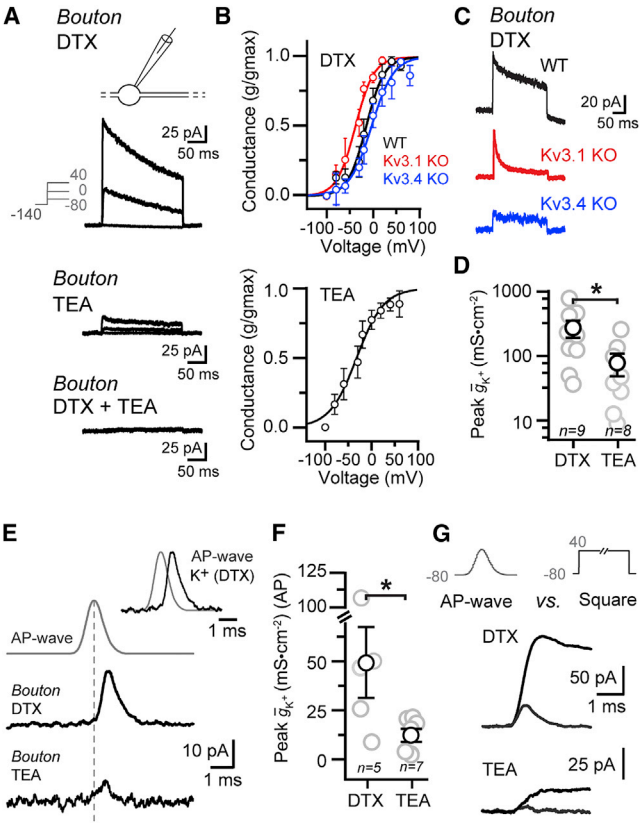

Figure 5. Fast-Activating K_v Channel Types at Boutons

(A) Depolarization-evoked K^+ currents, recorded in cell-attached patches from separate boutons, in the presence of DTX (200 nM), TEA (1 mM), or both DTX and TEA.

(B) Activation curves of fast-activating K^+ currents recorded in bouton patches in either DTX or TEA, fit with Boltzmann functions (r^2 = 0.88, 0.88, and 0.99 for WT, K_v3.1 KO, and K_v3.4 KO, respectively in DTX, and r^2 = 0.76 for TEA).

(C) Comparison of fast-activating K^+ currents recorded in DTX in a WT, K_v3.1 KO, or K_v3.4 KO mouse, evoked by a depolarizing pulse to a maximally activating potential.

(D) Summary data show peak K^+ conductance density, derived from maximally activating fast currents measured in bouton patches, is greater for K_v3-mediated currents (DTX) relative to K_v1-mediated currents measured in TEA (*p = 0.04; Mann-Whitney test).

(E) K^+ currents evoked in bouton patches by an AP-like command waveform (800 μs half-width; AP peak +30 mV; shown in gray) in either DTX or TEA. The peak of the depolarizing voltage command is indicated by the dotted line.

(F) Summary data from cell-attached recordings from boutons showing currents evoked by an AP-like waveform from a physiological resting membrane potential in DTX were substantially larger than those measured in TEA (*p = 0.03; Mann-Whitney test).

(G) Superimposed K^+ currents measured in the same bouton, evoked by an AP-like waveform or a square pulse to a maximally activating potential in an interleaved fashion. In separate patches, currents were recorded either in DTX or TEA.

In summary plots, mean values (±SEM) are shown in black, red, or blue. See also Figures S5–S7.

AP Duration Is Shaped by the Local Availability of K_v3-Mediated Currents

From our patch measurements, the peak K_v-mediated $\bar{g}_{K^+}$ varied considerably from bouton to bouton (Figure 5D) and was significantly greater in boutons with respect to interconnecting shaft regions (Figure 4D), suggesting that the relative availability of K_v3 current may be an underlying factor in the local determination of AP duration. We returned to compartmental modeling to systematically explore how the distribution of K_v3-mediated currents at boutons may affect local spike repolarization. We focused on width changes of propagating APs in the shaft due to the predictability of distance-dependent duration changes observed experimentally (Figure 1J). We found that a uniform K_v3-mediated conductance at boutons resulted in little change in AP duration throughout the axon shaft test region (Figure S7A). However, increasing K_v3 conductance density at the test bouton relative to surrounding boutons led to a more rapid AP that broadened as the spike propagated into the shaft (Figures S7A, S7C, and S7D). Spike broadening in the shaft was enhanced by an accompanying increase in GR at the bouton (Figures S7A and S7C–S7E), a factor that multiplied the effect of K_v3 conductance density on AP duration at the test site. Thus, the variable availability of K_v3 current at boutons can impart local changes in AP width, an effect amplified by impedance mismatches dictated by differential axon geometry.

Bouton-Specific Control of AP Duration by Clustered K_v3 Organization

Our findings suggest that the clustered arrangement of K_v3 channels at boutons imparts local tuning of spike repolarization between release sites in SC axons. If so, AP duration should be set by K_v3 channels immediately local to an individual bouton and resistant to alteration in channel availability at other presynaptic sites. To experimentally determine the spatial extent by which K_v3 channels influence AP repolarization, we used 2P laser uncaging (2PLU) of the photolyzable K^+ channel blocker RuBi-4AP (Zayat et al., 2003) to locally inhibit fast-activating K^+ channels at individual boutons and probe for changes in spike duration using simultaneous 2P VSD imaging.

When laser pulses were directed near the periphery of targeted boutons, photo-liberated 4AP was sufficient to induce AP broadening (Figures 6A and 6B; also observed in mice >6 weeks; 32°C; 129.0% ± 12.2% increase from matched control; n = 9; p = 0.03; paired t test). This effect began to reverse rapidly (Figure 6B), likely owing to the small focal volume of 2P excitation and diffusion. When uncaging points were repositioned slightly away from the target bouton, 2PLU failed to induce spike broadening (Figure 6C), indicating that the area of 4AP-mediated channel block was likely constrained to a region encompassing approximately a single bouton. These results confirm that K^+ channels in the immediate vicinity of an individual bouton shape spike duration at that site. If the rate of AP repolarization is determined at an individual bouton, then it is expected that broadening in one bouton would not be reflected at nearby boutons. To address this question, we recorded APs in interleaved trials from two boutons located in close proximity on the same branch and used 2PLU of RuBi-4AP to induce a substantial increase in spike width (≥15% of control) at the first site (Figure 6D). Despite an alteration at the test location, we found that spike broadening was highly reduced in orthodromic APs measured at the second site (Figure 6E). This result could be recapitulated in our compartmental model by simulating the loss

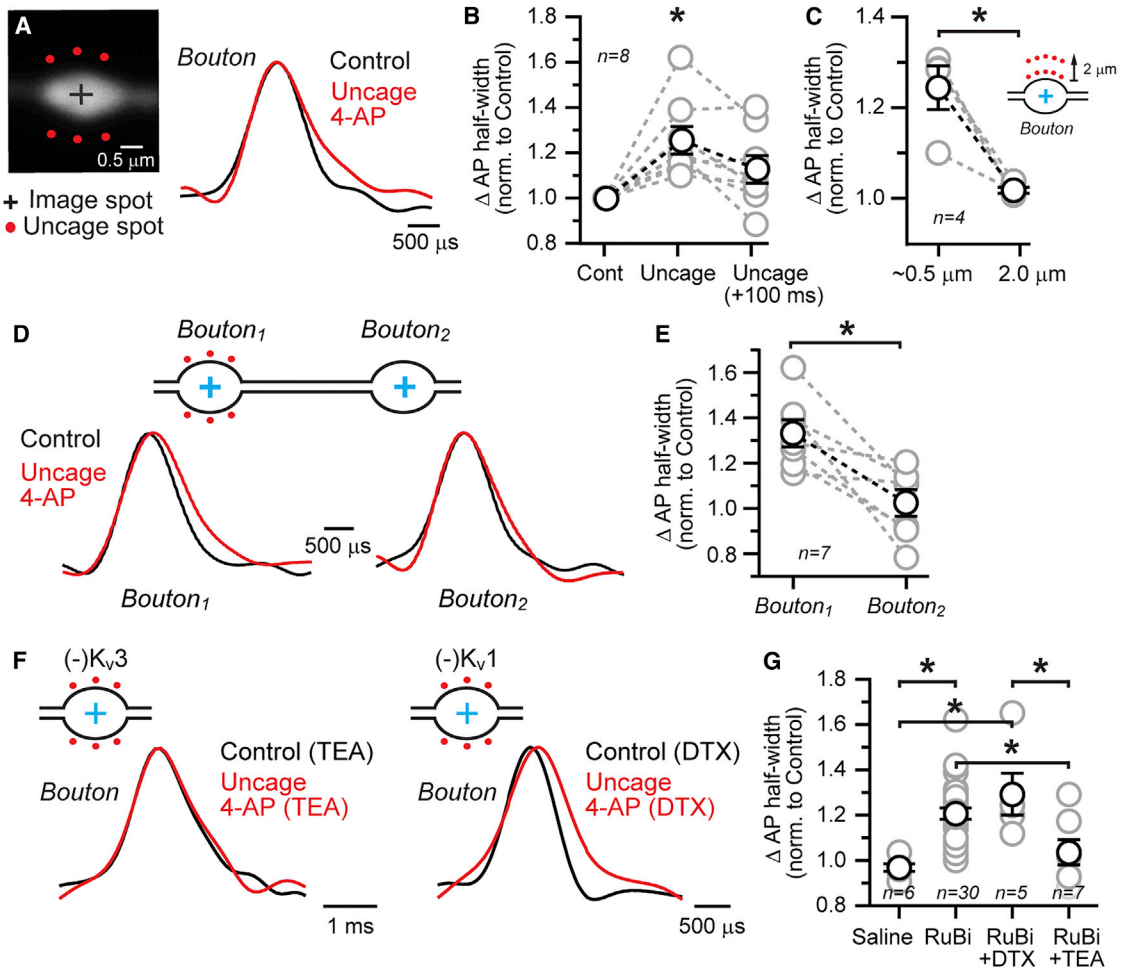

Figure 6. Local Control of AP Width at Individual Boutons

(A) Image of a bouton targeted for 2P VSD imaging and 2PLU of bath-applied RuBi-4AP (300 μM). APs were recorded in control and briefly following (20 ms) RuBi-4AP uncaging near the periphery of the target bouton (~0.5 μm).

(B) AP broadening induced at boutons following 2PLU of RuBi-4AP decayed rapidly with time after uncaging (*$p < 0.05$).

(C) Moving the location of uncaging points lateral to the target bouton (~2 μm; perpendicular to the axis of axon) eliminates the effect of spike broadening induced by photolysis of RuBi-4AP (*$p = 0.02$).

(D) APs measured iteratively in two nearby boutons on the same axon branch before and briefly following RuBi-4AP uncaging at the target bouton.

(E) Spike broadening induced by Rubi-4AP uncaging at target boutons was highly reduced in orthodromic APs measured at nearby boutons (*$p = 0.009$; mean distance between boutons 12.6 ± 2.2 μm). In this analysis, we used test boutons that were substantially broadened by 2PLU of Rubi-4AP (≥15%).

(F) APs measured in boutons before and briefly following Rubi-4AP uncaging in a background of bath applied DTX (200 nM) or TEA (500 μM).

(G) Group data comparison showing the effect of 2PLU of Rubi-4AP on AP duration in control, DTX, or TEA. 2PLU pulses without 4AP failed to induce a change in spike duration (*$p < 0.05$).

Significance determined with one-way ANOVA followed by Tukey's multiple comparison test (B and G) or with a paired t test (C and E). In summary graphs, mean values (±SEM) are shown in black with data from individual patches in gray.

See also Figure S7.

of $\overline{g}_{K^+}$ at the test bouton (Figure S7F), indicating that the local availability of K_v channels is a critical determinate of this effect. Together, these results confirm that AP repolarization is shaped in a highly localized manner, thus allowing boutons to individually tune spike width independent of other release sites.

4AP inhibits both K_v1 and K_v3 channels (Coetzee et al., 1999), though K_v3 channels are particularly sensitive to 4AP block (Alle et al., 2011; Ishikawa et al., 2003; Southan and Robertson, 2000). To examine for the specific role of K_v3 channels in 2PLU-induced AP broadening, we repeated RubBi-4AP uncaging experiments including TEA in the bath solution to occlude K_v3 channels. In this condition, spike duration was relatively insensitive to Rubi-4AP uncaging (Figures 6F and 6G). A similar result was also observed in matched comparisons made at the same bouton, where spike broadening was induced by RuBi-4AP uncaging prior to TEA application (123% ± 6.0% and 107% ± 6.2% of control AP duration; control and TEA, respectively; $n = 5$; $p < 0.05$; paired t test). In contrast, Rubi-4AP uncaging continued to

induce spike broadening in DTX (Figures 6F and 6G). Thus, the local availability of K_v3 channels governs spike repolarization rate at individual boutons in SC axons, with K_v1 channels playing an insignificant role. Although we cannot rule out the possibility that low abundance of K_v1-mediated current was insufficient to impart local control of AP repolarization, we found that substituting slower delayed rectifier K^+ channels for K_v3 in our model greatly increased the apparent length constant of spike broadening following the simulated uncaging condition (Figure S7G). This suggests that the biophysical features of K_v3 channels are particularly well-adapted for spatially restricted control of spike repolarization in SC axons.

Spike Width Differences Contribute to Heterogeneity of Release Efficacy

To examine how local determination of spike width at SC boutons contributes to control of neurotransmission, we measured AP-evoked $GABA_A$ autoreceptor (pre-$GABA_AR$) currents (Pouzat and Marty, 1999). In voltage-clamped cells, brief depolarizing pulses (0.5–1.0 ms; +10 mV) elicited unclamped spikes at the soma, followed immediately by a transient synaptic current mediated by the evoked release of GABA and subsequent binding to pre-$GABA_ARs$ expressed on the axon (Figures 7A and 7B). Autoreceptor currents were also resolved in simultaneous axon-attached recordings from boutons, showing rapid kinetics and inhibition by the $GABA_AR$ antagonist GABAzine (Figures 7A and 7B). Following block of K_v3 channels with TEA (1 mM) to induce AP broadening, we measured an increase in the peak amplitude of the pre-$GABA_AR$ current at the axon recording site (136.3% ± 14.1% of control amplitude; n = 9; p = 0.03; Wilcoxon matched-pairs test) as well as a delay in the time to peak current (134.2% ± 10.3% of control; n = 9; p = 0.02; paired t test) (Figure 7C). Thus, like at other synapses, spike width at SC boutons affects not only the release probability but also synaptic delay (Borst and Sakmann, 1999; Boudkkazi et al., 2011; Sabatini and Regehr, 1996, 1997).

In many cell types, including SCs, release probability varies between presynaptic sites, in part reflecting differences in vesicle docking sites and Ca_v channel abundance and organization (Holderith et al., 2012; Sheng et al., 2012; Trigo et al., 2012). Local regulation of AP duration between boutons may also contribute to release heterogeneity, but this possibility remains largely unexplored. We observed a wide range of paired-pulse ratio (PPR) values (0.52–1.58; 50 ms interstimulus interval) across all bouton recordings (mean PPR, 1.05 ± 0.04; n = 24), similar to population data from paired recordings of interconnected SCs (Christie et al., 2011). Using multisite electrode recording at boutons located on different axon branches, we observed non-uniformity in the PPR of AP-evoked pre-$GABA_AR$ currents (Figure 7D; normalized PPR [$PPR_{bouton2}/PPR_{bouton1}$], 123.0% ± 4.6%; n = 7 pairs), confirming that release efficacy varies along the axon of SCs (Pulido et al., 2015). Furthermore, this observation indicates that the pre-$GABA_AR$ responses recorded at each axon site must be mediated by the activity of largely non-overlapping synaptic populations.

To study how local control of AP repolarization may contribute to release heterogeneity, we constrained the area of K_v channel block with targeted 2PLU of Rubi-4AP to a small subregion of the axon (~15 μm in length) surrounding the axon recording site (Figure 7E). Uncaging induced both a prolongation of the AP recorded at the bouton test site (130.3% ± 10.6% of control width; p = 0.006; n = 7; paired t test) and an increase in pre-$GABA_AR$ amplitude and synaptic delay (143.7% ± 18.6% and 135.0% ± 13.1% of control; amplitude and time to peak, respectively; both $p < 0.05$; n = 7; Wilcoxon matched-pairs tests; Figure 7E). Consistent with an alteration in strength of neurotransmission, uncaging also produced a change in PPR at the axon site (Figure 7F); however, the PPR of the somatic current remained unchanged (Figure 7F), likely due to sampling of abundant pre-$GABA_AR$ activity from non-target axon regions. Therefore, by locally setting spike duration, and hence the AP-evoked Ca^{2+} entry (Rowan et al., 2014), the availability of K_v3 channels at individual SC boutons must be a contributing factor to differences in release efficacy and timing among synapses on the same axon.

DISCUSSION

We show that in axons of cerebellar SCs, spike duration varies within the axon, including among neighboring boutons on the same branch. Local modulation of spike waveform results from a non-uniform organization of voltage-gated K^+ channels, including clustering of fast-activating K_v3 channels at presynaptic sites. Such organization yields a powerful adaptive property allowing individual release sites to locally shape the duration of a propagating spike, dependent on the local abundance of K_v3 channels and separate of other sites. This feature allows for tuning of neurotransmission in a near synapse-by-synapse manner, thus contributing to the heterogeneity of release, an important factor permitting flexibility in neural circuit signaling.

Local Determination of AP Duration in Boutons

The perception that APs propagate as a static waveform throughout the entire axon has been continuously challenged in a variety of neuron types in both invertebrates (Lin, 2012; Nagano and Cooke, 1987) and vertebrates (Kawaguchi and Sakaba, 2015; Kole et al., 2007). Our results indicate that although spikes are reliably transmitted in SC axons, the duration of the AP frequently deviated from one presynaptic site to the next. This phenomenon may also occur in other neuron types. For example, whole-cell measurements from hippocampal mossy fiber boutons show considerable variation in spike duration within the sample population (i.e., 254–533 μs) (Geiger and Jonas, 2000), although direct observations from multiple sites on a single axon are lacking. In this report, we used multisite axon recording and found significant variability in spike duration within the axon of individual SCs, including nearby boutons on the same branch.

Control of spike signaling is often partitioned in axons and dependent on non-uniform distributions of voltage-gated ion channels, including K^+ channels (Debanne et al., 2011; Trimmer, 2015). In SC axons, our functional mapping revealed fast-activating K^+ channels at presynaptic boutons that were largely excluded from shafts, indicating a high degree of specificity in their subcellular organization. That the length constant of AP broadening in the shaft was less than that expected for purely

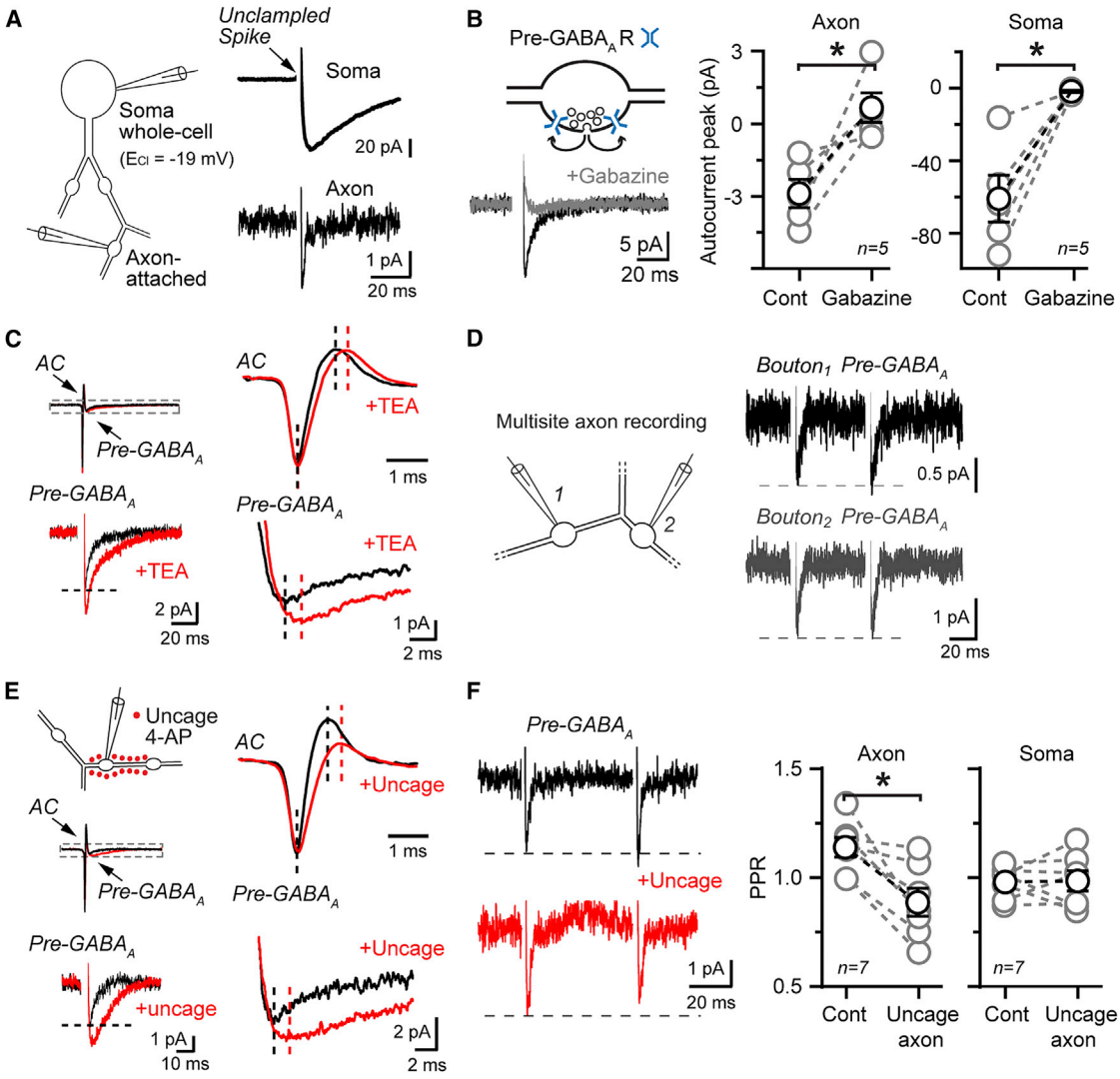

Figure 7. Local Control of AP Width Contributes to Heterogeneity of Release

(A) Autocurrents recorded at the soma in voltage-clamp mode following brief depolarization as well as at the axon during simultaneous cell-attached recording in the loose-seal configuration. The unclamped spike elicited at the soma and action current at the axon were blanked for clarity.

(B) Autocurrent response measured at the axon in control and in gabazine (20 μM). Summary data show that the autoreceptor current, measured at either at the axon or soma, was $GABA_AR$ mediated.

(C) At the axon, TEA induced an increase in the peak-to-peak duration of the action current and a corresponding increase in the amplitude of the synaptic pre-$GABA_AR$ response. In the magnified view on the right, dashed lines show that the time-to-peak response of the pre-$GABA_AR$ current in TEA was also delayed relative to the control response.

(D) Multisite recording of pre-$GABA_AR$ currents from the same axon. The dotted line indicates the amplitude of the first response for paired stimuli.

(E) Targeted 2PLU of Rubi4AP (300 μM) over a small region of axon centered at the recording location (20–30 pulses; over ~15 μm of axon). Currents corresponding to the AP and pre-$GABA_AR$ response are shown for control and uncaging conditions.

(F) $GABA_AR$ responses following two closely timed APs in both control and uncaging conditions from the same recording location. Summary plots show uncaging induced changes in PPR at the axon recording site, but not at the soma (*p = 0.007; paired t test).

For all summary graphs, mean values (±SEM) are shown in black with data from individual patches in gray outline.

passive signals, including those with a high frequency content such as an AP, indicates that the organization of active currents is paramount for this effect.

APs are autoregenerative signals with repolarization largely determined by K^+ currents. By clustering K^+ channels at presynaptic locations in SCs, AP duration is shaped on a very local scale dependent on K^+ currents immediately available at an individual bouton. In this way, spike broadening induced by focal block of K^+ channels in a target bouton is highly reduced in the orthodromic spike measured at near-neighbor sites. Comparatively, focally induced AP broadening in axons of L5 pyramidal cells (Kole et al., 2007) and hippocampal CA3 neurons (Sasaki

et al., 2011) may extend for much greater distances, perhaps owing to differences in the types and organization of K^+ channels. Although, in L5 pyramidal cells regulation of AP repolarization by DTX-sensitive K_v1 channels in axon collaterals may occur in a more localized manner (Foust et al., 2011), suggesting that local shaping of APs may be a generalizable feature of unmyelinated axon regions.

K_v3-Mediated Currents in Boutons

Following pharmacological block of K_v3, AP duration was much more uniform in the axons of SCs, indicating that the organization of this fast-activating channel type is a key parameter permitting heterogeneity of spike repolarization within individual axons. In cell-attached patches from SC boutons, we recorded K^+ currents mediated by both K_v1- and K_v3-type channels. The same current complement has also been reported for the pinceau axon specializations of cerebellar basket cells (Southan and Robertson, 2000), a closely related interneuron type in the molecular layer (Sultan and Bower, 1998). Although currents mediated by both K_v1 and K_v3 channels contribute to AP repolarization in the boutons of some cell types (Hoppa et al., 2014; Ritzau-Jost et al., 2014), we found that the conductance carried by K_v3-mediated currents predominates when driven by an AP-like waveform from a physiological resting membrane potential, likely explaining why AP repolarization is determined by this channel type rather than K_v1 (Rowan et al., 2014). At hippocampal mossy fiber boutons, fast-opening K_v3 channels outpace other channel types to direct spike repolarization (Alle et al., 2011). However, we did not measure an appreciable difference in K_v1 and K_v3 activation rates at suprathreshold potentials, suggesting that relative availability, rather than rapid and efficient opening, is the determinate factor guiding K^+ channel participation in AP repolarization in SC axons. The reasons for these cell-type-specific differences are not clear; however, neurons may achieve state-dependent control of K^+ channels by differential phosphorylation or assembly with accessory subunits to precisely determine excitability (Macica and Kaczmarek, 2001; Rettig et al., 1994; Ritter et al., 2012).

In myelinated axons, K^+ channels are known to cluster in macromolecular complexes at nodes of Ranvier and, in the case of K_v3, are dependent on interactions with the membrane-bound proteins (Devaux et al., 2003). Our work points to differences in the current density of clustered K_v3 channels at release sites as the underlying factor contributing to variability in spike duration in SC axons. The trafficking, sequestration, and complexing of K^+ channels in unmyelinated axons are, in general, poorly understood (Trimmer, 2015), and hence the mechanistic underpinnings resulting in the differential expression density of K_v3 at SC boutons remain unclear. It is important to note that variability in our patch measurements may stem from sampling random channel clusters on the membrane of individual boutons. In fact, fast-activating K^+ currents weren't apparent in many bouton patches, an observation that was more common following pharmacological isolation of K_v1 and K_v3 currents, suggestive of partitioning of these channels types. However, microclustering of K_v3 channels within a bouton would not necessarily prevent local shaping of APs, as the average conductance density across the bouton would still likely affect spike duration given the small and uniform nature of bouton morphology. Whether differences in K_v3 channel abundance at other synapses including mossy fiber boutons (Alle et al., 2011) are sufficient to impart a change in AP duration is unknown.

K_v3 Channel Types

K_v3 channel gating properties vary with subunit composition, including the voltage dependence of activation (Baranauskas et al., 2003). Using KO mice, we identify diminished K_v3-mediated current density in boutons as well as phenotypic alteration in activation voltage accompanying loss of either $K_v3.1$ or $K_v3.4$, indicating that these subunits are constituent components of K_v3 channels in SC axons. $K_v3.4$ channels have a hyperpolarized activation voltage that is amenable to efficient recruitment during an AP (Baranauskas et al., 2003), perhaps contributing to the high K^+ flux required for local tuning of AP waveform, as indicated by our modeling. Interestingly, replacing K_v3 channels with a slower delayed rectifier type in our simulations increased the apparent length constant of AP broadening, indicating that the biophysical features of K_v3 channels are well-suited to support local control of AP shape. As K_v3 subunits can co-assemble to form functional channels with intermediate gating features (Coetzee et al., 1999), it may be that the K_v3 subunit composition is differentially regulated across SC release sites, determined by development or plasticity, imparting differential control of local spike duration. However, we did not systematically explore the subunit stoichiometry of K_v3 channels in SC axons.

Axon Geometry and AP Duration

Ultrastructural inspection of SC axons revealed a compact electrotonic structure amenable to local spike shaping. SC axons are thin, include frequent geometric swelling at presynaptic boutons, and are likely unmyelinated given the conspicuous absence of oligodendrocyte ensheathment. Though the varicose morphology of boutons may impose a substantial electrical load, or impedance, to an invading AP (Goldstein and Rall, 1974; Lüscher and Shiner, 1990), our experimental and modeling data indicate that it is unlikely that geometry alone distorts the waveform to sufficiently account for the variability in AP duration we measured in individual SCs. Similar to the unmyelinated axons of CA3 pyramidal cells in the hippocampus (Shepherd and Harris, 1998), the geometric difference between boutons and their adjoining shafts in SCs is quite small. However, our modeling results indicate that bouton geometry may work in combination with the variable expression density of K_v3 channels to amplify changes in AP duration. Yet we found no predictable relationship between AP duration and bouton size, indicating that the organization of K^+ channels may be regulated independent of morphological features.

Local Control of AP Duration and Neurotransmission

As shown previously in SC boutons, spike repolarization rate directs Ca_v channel opening and Ca^{2+} influx, and therefore determines release efficacy (Rowan et al., 2014). In this report, using axon-targeted recording of pre-$GABA_AR$-mediated currents, we find intersynaptic variability of release probability that can be locally modified by the duration of the AP at a bouton release site. Release heterogeneity, even within individual axons of SCs,

depends on many structural and molecular properties, including the number of vesicle docking sites (Pulido et al., 2015; Trigo et al., 2012), whose attributes likely stem from the abundance of presynaptic Ca^{2+} channels that scale with bouton size, similar to other small central synapses (Holderith et al., 2012).

We propose that variation in AP-evoked Ca^{2+} entry may not only reflect variability in Ca_v channel number but also underlying differences in AP width, and may be set independent of bouton size (Ermolyuk et al., 2012) if Ca_v and K_v channel abundance is set independently. However, adaptive plasticity may drive changes in AP duration through modification of presynaptic K^+ channels in lockstep with the organization and abundance of Ca_v channels to maintain release probability in a useful signaling range (Hoppa et al., 2012, 2014), indicating a concerted interplay between spike repolarization and Ca^{2+} channel availability and regulation. AP broadening is also well-suited to affect synaptic timing (Boudkkazi et al., 2011), as Ca^{2+} entry mainly occurs during spike repolarization (Sabatini and Regehr, 1996, 1997). Thus, local control of AP duration at individual release sites is likely an important feature contributing to heterogeneity in both the timing and strength of neurotransmission from sites on the same axon, representing an additional element contributing to the diverse coding range of synapses necessary for many computations. The absolute relationship between AP repolarization, Ca^{2+} entry, and effect on neurotransmission likely requires additional investigation, as $GABA_AR$ receptor saturation at SC synapses will blunt the amplitude change of the synaptic response following an increase in release probability (Pulido et al., 2015). Additionally, a clustered organization of fast-activating K^+ channels may be metabolically advantageous, as the energetic cost of AP signaling is thought to consume substantial amounts of ATP to maintain and restore ionic gradients (Alle et al., 2009; Carter and Bean, 2009). By limiting K^+ channel activity to synapses, spike repolarization may be modulated in a more energy-efficient manner.

EXPERIMENTAL PROCEDURES

Experimental Procedures are described in detail in the Supplemental Experimental Procedures. All animal procedures were approved by the Max Planck Florida Institute for Neuroscience Animal Care and Use Committee.

Presynaptic Recordings from SC Axons

SC recordings were performed in cerebellar slices prepared from C57Bl/6 mice (post-natal day [P]15–P54) at 24°C or 32°C. Axonal loose-seal or channel recordings were guided with fluorescently labeled pipettes to axonal sites of interest. The voltage-sensitive dye di-2-AN-(F)EPPTEA (30 μM; L. Loew; University of Connecticut Health Center) was included in the intracellular solution for voltage imaging experiments. All imaging was performed with a 2P laser scanning microscope (Ultima; Bruker Corp.) using an Olympus upright microscope (BX51WI) and objective (60×, 1.0 NA), and excitation provided by a mode-locking Ti:sapphire laser (Chameleon Ultra II; Coherent Inc.).

RuBi-4AP Uncaging

The photolyzable voltage-gated K^+ channel blocker bis(2,2′-Bipyridine-N,N') bis(4-aminopyridine-N1) ruthenium (RuBi-4AP; Abcam) (Zayat et al., 2003) was recirculated in the bath solution and uncaged with rapid pulses (750 nm; 2 ms) from a second mode-locked laser (Chameleon Ultra II; Coherent Inc.). Pulses were modulated with a Pockels cell. Uncaging sites were directed within close proximity (~0.5 μm) of targeted boutons using a set of galvanometer mirrors independent of the imaging path, allowing for rapid positioning of the photolysis beam.

Electron Microscopy and 3D Reconstructions

Axons of SCs were ultrastructurally reconstructed from P19 mice using aldehyde-fixed cerebellar tissue. Ultrathin serial sections (~70 nm) were imaged with a transmission electron microscope (Tecnai G2; FEI) at 80 kV. Image stacks were manually inspected to identify axon fragments of SC interneurons. Areas containing SC axons were cropped for reconstruction and analysis using RECONSTRUCT software (Fiala, 2005).

Compartmental Model and Simulations

Simulations of AP propagation were performed using the NEURON environment (Hines and Carnevale, 2001) and analyzed using MATLAB (Mathworks). Compartmental model morphology was set to represent a simplified SC axon. Simulations included both voltage-gated Na^+ and K^+ channels implemented as Hodgkin-Huxley-type models.

Intracranial Viral Injections

Stereotactic injections were performed on mice (P18–P28) under anesthesia. Viruses were injected into the cerebellar vermis. After allowing 14–42 days for expression, animals were sacrificed and the cerebellum used for acute slice preparation.

SUPPLEMENTAL INFORMATION

Supplemental Information includes Supplemental Experimental Procedures, seven figures, and one table and can be found with this article online at http://dx.doi.org/10.1016/j.neuron.2016.05.035.

AUTHOR CONTRIBUTIONS

Conceptualization, M.J.M.R. and J.M.C.; Methodology, M.J.M.R. and J.M.C.; Investigation, M.J.M.R., G.D., J.J.Y., and N.K.; Writing – Original Draft, M.J.M.R. and J.M.C.; Funding Acquisition, M.J.M.R. and J.M.C.; Supervision, J.M.C.

ACKNOWLEDGMENTS

We thank Chris McBain (NICHD), Yishai Elyada (Hebrew University), and the members of the J.M.C. lab for their helpful discussions and comments during the preparation of this manuscript. Synaptophysin plasmid DNA was generated by Hiroki Tanaguchi and Andre Steinecke (MPFI). Fluorescently tagged $K_v3.4$ plasmid DNA was provided by Tatiana Tkatch (Lithuanian University of Health Sciences) and D. James Surmeier (Northwestern). Plasmids were prepared with help from the Max Planck Florida Molecular Core Facility. This work was supported by the Max Planck Society, the Max Planck Florida Institute for Neuroscience, NIH grant NS083127 (M.J.M.R.), and NIH grant NS083894 (J.M.C).

Received: September 21, 2015
Revised: March 13, 2016
Accepted: May 23, 2016
Published: June 23, 2016

REFERENCES

Acker, C.D., Yan, P., and Loew, L.M. (2011). Single-voxel recording of voltage transients in dendritic spines. Biophys. J. *101*, L11–L13.

Alle, H., Roth, A., and Geiger, J.R. (2009). Energy-efficient action potentials in hippocampal mossy fibers. Science *325*, 1405–1408.

Alle, H., Kubota, H., and Geiger, J.R. (2011). Sparse but highly efficient Kv3 outpace BKCa channels in action potential repolarization at hippocampal mossy fiber boutons. J. Neurosci. *31*, 8001–8012.

Babila, T., Atlan, H., Fromer, I., Schwalb, H., Uretzky, G., and Lichtstein, D. (1990). Volume regulation of nerve terminals. J. Neurochem. *55*, 2058–2062.

Baranauskas, G., Tkatch, T., Nagata, K., Yeh, J.Z., and Surmeier, D.J. (2003). Kv3.4 subunits enhance the repolarizing efficiency of Kv3.1 channels in fast-spiking neurons. Nat. Neurosci. *6*, 258–266.

Borst, J.G., and Sakmann, B. (1999). Effect of changes in action potential shape on calcium currents and transmitter release in a calyx-type synapse of the rat auditory brainstem. Philos. Trans. R. Soc. Lond. B Biol. Sci. *354*, 347–355.

Boudkkazi, S., Fronzaroli-Molinieres, L., and Debanne, D. (2011). Presynaptic action potential waveform determines cortical synaptic latency. J. Physiol. *589*, 1117–1131.

Carter, B.C., and Bean, B.P. (2009). Sodium entry during action potentials of mammalian neurons: incomplete inactivation and reduced metabolic efficiency in fast-spiking neurons. Neuron *64*, 898–909.

Christie, J.M., Chiu, D.N., and Jahr, C.E. (2011). Ca(2+)-dependent enhancement of release by subthreshold somatic depolarization. Nat. Neurosci. *14*, 62–68.

Coetzee, W.A., Amarillo, Y., Chiu, J., Chow, A., Lau, D., McCormack, T., Moreno, H., Nadal, M.S., Ozaita, A., Pountney, D., et al. (1999). Molecular diversity of K+ channels. Ann. N Y Acad. Sci. *868*, 233–285.

Debanne, D., Campanac, E., Bialowas, A., Carlier, E., and Alcaraz, G. (2011). Axon physiology. Physiol. Rev. *91*, 555–602.

Devaux, J., Alcaraz, G., Grinspan, J., Bennett, V., Joho, R., Crest, M., and Scherer, S.S. (2003). Kv3.1b is a novel component of CNS nodes. J. Neurosci. *23*, 4509–4518.

Dodson, P.D., and Forsythe, I.D. (2004). Presynaptic K+ channels: electrifying regulators of synaptic terminal excitability. Trends Neurosci. *27*, 210–217.

Engel, D., and Jonas, P. (2005). Presynaptic action potential amplification by voltage-gated Na+ channels in hippocampal mossy fiber boutons. Neuron *45*, 405–417.

Ermolyuk, Y.S., Alder, F.G., Henneberger, C., Rusakov, D.A., Kullmann, D.M., and Volynski, K.E. (2012). Independent regulation of basal neurotransmitter release efficacy by variable Ca^2+ influx and bouton size at small central synapses. PLoS Biol. *10*, e1001396.

Fiala, J.C. (2005). Reconstruct: a free editor for serial section microscopy. J. Microsc. *218*, 52–61.

Foust, A.J., Yu, Y., Popovic, M., Zecevic, D., and McCormick, D.A. (2011). Somatic membrane potential and Kv1 channels control spike repolarization in cortical axon collaterals and presynaptic boutons. J. Neurosci. *31*, 15490–15498.

Geiger, J.R., and Jonas, P. (2000). Dynamic control of presynaptic Ca(2+) inflow by fast-inactivating K(+) channels in hippocampal mossy fiber boutons. Neuron *28*, 927–939.

Goldstein, S.S., and Rall, W. (1974). Changes of action potential shape and velocity for changing core conductor geometry. Biophys. J. *14*, 731–757.

Hines, M.L., and Carnevale, N.T. (2001). NEURON: a tool for neuroscientists. Neuroscientist *7*, 123–135.

Ho, C.S., Grange, R.W., and Joho, R.H. (1997). Pleiotropic effects of a disrupted K+ channel gene: reduced body weight, impaired motor skill and muscle contraction, but no seizures. Proc. Natl. Acad. Sci. USA *94*, 1533–1538.

Holderith, N., Lorincz, A., Katona, G., Rózsa, B., Kulik, A., Watanabe, M., and Nusser, Z. (2012). Release probability of hippocampal glutamatergic terminals scales with the size of the active zone. Nat. Neurosci. *15*, 988–997.

Hoppa, M.B., Lana, B., Margas, W., Dolphin, A.C., and Ryan, T.A. (2012). $\alpha 2\delta$ expression sets presynaptic calcium channel abundance and release probability. Nature *486*, 122–125.

Hoppa, M.B., Gouzer, G., Armbruster, M., and Ryan, T.A. (2014). Control and plasticity of the presynaptic action potential waveform at small CNS nerve terminals. Neuron *84*, 778–789.

Hu, H., and Jonas, P. (2014). A supercritical density of Na(+) channels ensures fast signaling in GABAergic interneuron axons. Nat. Neurosci. *17*, 686–693.

Ishikawa, T., Nakamura, Y., Saitoh, N., Li, W.B., Iwasaki, S., and Takahashi, T. (2003). Distinct roles of Kv1 and Kv3 potassium channels at the calyx of Held presynaptic terminal. J. Neurosci. *23*, 10445–10453.

Kawaguchi, S.Y., and Sakaba, T. (2015). Control of inhibitory synaptic outputs by low excitability of axon terminals revealed by direct recording. Neuron *85*, 1273–1288.

Kole, M.H., Letzkus, J.J., and Stuart, G.J. (2007). Axon initial segment Kv1 channels control axonal action potential waveform and synaptic efficacy. Neuron *55*, 633–647.

Leão, R.M., Kushmerick, C., Pinaud, R., Renden, R., Li, G.L., Taschenberger, H., Spirou, G., Levinson, S.R., and von Gersdorff, H. (2005). Presynaptic Na+ channels: locus, development, and recovery from inactivation at a high-fidelity synapse. J. Neurosci. *25*, 3724–3738.

Lien, C.C., and Jonas, P. (2003). Kv3 potassium conductance is necessary and kinetically optimized for high-frequency action potential generation in hippocampal interneurons. J. Neurosci. *23*, 2058–2068.

Lin, J.W. (2012). Spatial variation in membrane excitability modulated by 4-AP-sensitive K+ channels in the axons of the crayfish neuromuscular junction. J. Neurophysiol. *107*, 2692–2702.

Lüscher, H.R., and Shiner, J.S. (1990). Computation of action potential propagation and presynaptic bouton activation in terminal arborizations of different geometries. Biophys. J. *58*, 1377–1388.

Macica, C.M., and Kaczmarek, L.K. (2001). Casein kinase 2 determines the voltage dependence of the Kv3.1 channel in auditory neurons and transfected cells. J. Neurosci. *21*, 1160–1168.

Martina, M., Metz, A.E., and Bean, B.P. (2007). Voltage-dependent potassium currents during fast spikes of rat cerebellar Purkinje neurons: inhibition by BDS-I toxin. J. Neurophysiol. *97*, 563–571.

Nagano, M., and Cooke, I.M. (1987). Comparison of electrical responses of terminals, axons, and somata of a peptidergic neurosecretory system. J. Neurosci. *7*, 634–648.

Pouzat, C., and Marty, A. (1999). Somatic recording of GABAergic autoreceptor current in cerebellar stellate and basket cells. J. Neurosci. *19*, 1675–1690.

Pulido, C., Trigo, F.F., Llano, I., and Marty, A. (2015). Vesicular release statistics and unitary postsynaptic current at single GABAergic synapses. Neuron *85*, 159–172.

Pullarkat, P.A., Dommersnes, P., Fernández, P., Joanny, J.F., and Ott, A. (2006). Osmotically driven shape transformations in axons. Phys. Rev. Lett. *96*, 048104.

Rettig, J., Heinemann, S.H., Wunder, F., Lorra, C., Parcej, D.N., Dolly, J.O., and Pongs, O. (1994). Inactivation properties of voltage-gated K+ channels altered by presence of beta-subunit. Nature *369*, 289–294.

Ritter, D.M., Ho, C., O'Leary, M.E., and Covarrubias, M. (2012). Modulation of Kv3.4 channel N-type inactivation by protein kinase C shapes the action potential in dorsal root ganglion neurons. J. Physiol. *590*, 145–161.

Ritzau-Jost, A., Delvendahl, I., Rings, A., Byczkowicz, N., Harada, H., Shigemoto, R., Hirrlinger, J., Eilers, J., and Hallermann, S. (2014). Ultrafast action potentials mediate kilohertz signaling at a central synapse. Neuron *84*, 152–163.

Rowan, M.J., Tranquil, E., and Christie, J.M. (2014). Distinct Kv channel subtypes contribute to differences in spike signaling properties in the axon initial segment and presynaptic boutons of cerebellar interneurons. J. Neurosci. *34*, 6611–6623.

Sabatini, B.L., and Regehr, W.G. (1996). Timing of neurotransmission at fast synapses in the mammalian brain. Nature *384*, 170–172.

Sabatini, B.L., and Regehr, W.G. (1997). Control of neurotransmitter release by presynaptic waveform at the granule cell to Purkinje cell synapse. J. Neurosci. *17*, 3425–3435.

Sasaki, T., Matsuki, N., and Ikegaya, Y. (2011). Action-potential modulation during axonal conduction. Science *331*, 599–601.

Sasaki, T., Matsuki, N., and Ikegaya, Y. (2012). Targeted axon-attached recording with fluorescent patch-clamp pipettes in brain slices. Nat. Protoc. *7*, 1228–1234.

Segev, I., and Schneidman, E. (1999). Axons as computing devices: basic insights gained from models. J. Physiol. Paris *93*, 263–270.

Sheng, J., He, L., Zheng, H., Xue, L., Luo, F., Shin, W., Sun, T., Kuner, T., Yue, D.T., and Wu, L.G. (2012). Calcium-channel number critically influences synaptic strength and plasticity at the active zone. Nat. Neurosci. *15*, 998–1006.

Shepherd, G.M., and Harris, K.M. (1998). Three-dimensional structure and composition of CA3→CA1 axons in rat hippocampal slices: implications for presynaptic connectivity and compartmentalization. J. Neurosci. *18*, 8300–8310.

Southan, A.P., and Robertson, B. (2000). Electrophysiological characterization of voltage-gated K(+) currents in cerebellar basket and purkinje cells: Kv1 and Kv3 channel subfamilies are present in basket cell nerve terminals. J. Neurosci. *20*, 114–122.

Sultan, F., and Bower, J.M. (1998). Quantitative Golgi study of the rat cerebellar molecular layer interneurons using principal component analysis. J. Comp. Neurol. *393*, 353–373.

Svoboda, K. (2004). Do spines and dendrites distribute dye evenly? Trends Neurosci. *27*, 445–446.

Trigo, F.F., Sakaba, T., Ogden, D., and Marty, A. (2012). Readily releasable pool of synaptic vesicles measured at single synaptic contacts. Proc. Natl. Acad. Sci. USA *109*, 18138–18143.

Trimmer, J.S. (2015). Subcellular localization of K+ channels in mammalian brain neurons: remarkable precision in the midst of extraordinary complexity. Neuron *85*, 238–256.

Williams, S.R., and Wozny, C. (2011). Errors in the measurement of voltage-activated ion channels in cell-attached patch-clamp recordings. Nat. Commun. *2*, 242.

Wu, X.S., Sun, J.Y., Evers, A.S., Crowder, M., and Wu, L.G. (2004). Isoflurane inhibits transmitter release and the presynaptic action potential. Anesthesiology *100*, 663–670.

Yang, Y.M., and Wang, L.Y. (2006). Amplitude and kinetics of action potential-evoked Ca2+ current and its efficacy in triggering transmitter release at the developing calyx of Held synapse. J. Neurosci. *26*, 5698–5708.

Yeung, S.Y., Thompson, D., Wang, Z., Fedida, D., and Robertson, B. (2005). Modulation of Kv3 subfamily potassium currents by the sea anemone toxin BDS: significance for CNS and biophysical studies. J. Neurosci. *25*, 8735–8745.

Zayat, L., Calero, C., Alborés, P., Baraldo, L., and Etchenique, R. (2003). A new strategy for neurochemical photodelivery: metal-ligand heterolytic cleavage. J. Am. Chem. Soc. *125*, 882–883.